IET Renewable Power Generation

Special Issue Call for Papers

Be Seen. Be Cited.
Submit your work to a new IET special issue

Connect with researchers and experts in your field and share knowledge.

Be part of the latest research trends, faster.

Read more

The Institution of Engineering and Technology

Received: 5 January 2021 | Revised: 17 February 2021 | Accepted: 29 March 2021

IET Renewable Power Generation

DOI: 10.1049/rpg2.12183

The Institution of Engineering and Technology WILEY

ORIGINAL RESEARCH PAPER

The study on the anti-impact performance of the oscillating buoy with various air cushions

Ruiyin Song[1,2] | **Congjie Ren**[3] | **Xiao Ma**[4] | **Liyang Qiu**[4] | **Zuan Lin**[1]

[1] NingboTech University, Ningbo, China

[2] Ningbo Research Institute, Zhejiang University, Ningbo, China

[3] Zhejiang University of Science and Technology, Ningbo, China

[4] Zhejiang University, Ningbo, China

Correspondence
Congjie Ren, NingboTech University, Yinzhou District, Ningbo City, Zhejiang Province, China, 315100.
Email: 953454163@qq.com

Funding information
National Key R&D Program of China, Grant/Award Number: 2016YFC0300500; Major Science and Technology Research Projects of Ningbo, Grant/Award Number: 2017C110005; Scientific and Technological Major Project of Ningbo, Grant/Award Number: 2015C50061

Abstract

Violent waves in ocean sometimes cause huge shocks to the oscillating buoy and cause its damage. Improving the structure of buoy is a common method to reduce the impact of water on buoy. This paper focuses on how to reduce the peak impact force and improve the survivability of oscillating buoy in ocean environment. Considering the air layer between oscillating buoy and water surface, the impact of buoy into water is taken as the research point in the paper. The corresponding mathematical model is established, and the analysis shows that the air cushion can greatly reduce the peak impact force of buoy. The finite element model of buoy is established, and the constant velocity entry of a series of buoys with different air cushion structures is calculated. First of all, the air cushions with different shapes are compared, the qualitative analysis shows that the air cushion of cylindrical shape has the excellent anti-impact performance. Then, the air cushion structure with different volume was analysed, and the influence of different air cushion volume on the peak impact force of buoy entering water was quantified. It is concluded that the effect of reducing peak of air cushion increases with the increase of air cushion volume. Furthermore, a test bench for the impact of buoy into water was set up for experiments, and similar conclusions were obtained. Besides, it is found that the improvement of the impact resistance of air cushion slows down as the volume of air cushion increases, and there is an upper limit which is positively correlated with the impact velocity of buoy.

1 | INTRODUCTION

As one of the renewable sources of energy that can supply part of the world's energy needs, the wave energy can be converted to electricity or other forms of usable energy. In recent years, many wave energy converter (WEC) have emerged and three main functional categories of WEC can be defined as follows: oscillating water column [1], wave activated or oscillating bodies (e.g. Oyster or Wave Roller) [2] and overtopping devices (e.g. Wave Dragon) [3]. The uncertainty of waves is large, and sometimes they produce a huge impact. For example, freak waves are much larger (at least twice as high) than waves in surrounding sea state. As opposed to regular storm waves, freak waves are highly limited to time and place, and difficult to predict and measure. The peak value of impact force is about 7–10 times higher than the average value, which has severe impact on mechanical parts of WEC or even destroys the wave energy conversion device [4–7]. Figure 1 shows the buoys installed by our research team in Xiangshan, Zhejiang Province, which was damaged due to excessive impact during a super typhoon.

In general, oscillating buoys have a lower draft depth, which increases their likelihood of leaving the surface of water. When it enters the water again especially in extreme sea conditions, the bottom of buoy is subjected to a strong slamming [8–11]. In addition, in order to avoid the destroy of the hazardous environments at sea, sometimes the buoys need to be suspended. It will also be subjected to the slamming when it begins to work again. The impact on the working performance and working life of buoys is very great because of its plastic deformation and fatigue failure. The entry of oscillating buoys into water

FIGURE 1 Damaged buoys

is a nonlinear and unsteady problem involving solid - air - water coupling [12–16]. In the early research, by analyzing and calculating the velocity potential of the flow field around the object, it shows the impact pressure acting on buoys changed with the time and space position. A lot of assumptions were made about the flow field in the derivation, and the existence of air was ignored [17–19]. In the process of buoy entries into water, because the bottom of buoy and the surface of water are particularly significant for the air escape restrictions, so in the study of buoy entry into water we need to consider the impact of air cushion. This paper studies the impact of buoy in the water from the perspective of air cushion, uses simulation software to calculate the entry of oscillating buoy into water, and analyses the changes in the air cushion of different structures when the buoy enters water and its influence on the peak of impact force. In addition, a comparative experiment was carried out by building a test bench, and the relationship between several factors of air cushion and its impact resistance was further studied. It is expected to provide a reference for the design of oscillating float in the future and enhance its robustness.

2 | THE THEORETICAL MODEL

2.1 | Calculation of peak impact before water entry

According to the 'Bad condition principle' in the engineering design, the vertical water entry should be considered first. Wagner's impulse slamming theory gives the calculation formula of impact pressure varying with time and space on the slamming surface [20]:

$$P(x) = \frac{1}{2}\rho v^2\left[\frac{\pi}{\beta(1-x^2/L^2)^{1/2}} - \frac{\frac{x^2}{L^2}}{1-\frac{x^2}{L^2}} + \frac{2\ddot{Z}}{v^2}\left(L^2-x^2\right)^{1/2}\right] \tag{1}$$

where ρ is the density of water, v is the water entering velocity, β is the angle between bottom surface and water surface, Z is the water entering depth, and L is the radius of structure on the water surface.

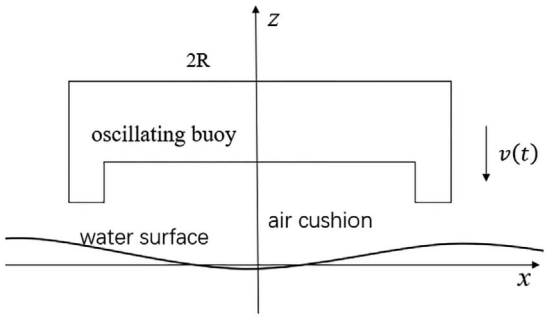

FIGURE 2 Simple buoy model before entering water

The maximum impact pressure is:

$$P_{max} = \frac{1}{2}\rho v^2\left(1+\frac{\pi^2}{4\beta}\right) \tag{2}$$

The peak of the impact pressure of the flat bottom structure in the experiment is obviously smaller than the peak of the impact pressure in the theoretical calculation. The important reason is that the air layer effect between structure and water surface is ignored in the theoretical calculation of the impact pressure of the flat bottom structure in the experiment. When entering water, part of the air between bottom and structure surface is 'captured' to form a sandwich air pad, which largely prevents the direct contact between structure and water surface, and slows down the impact of the surface on the structure. Therefore, the impact of air cushion on the peak pressure of flat bottom structure must be considered when studying the impact problem of flat bottom structure.

The buoy is generally an axisymmetric body with a simple shape. In order to facilitate research, the buoy is simplified into a two-dimensional model. The theoretical model of the air cushion of oscillating buoy before entering water is shown in the Figure 2. The bottom width of buoy is 2R and it falls at the velocity *v(t)*. In the model, it is assumed that air is a compressible ideal gas and satisfies the ideal equation

of state in the process of compression. In the calculation, the viscosity of air and water and the elasticity of plate are ignored.

During the buoy entry process, the movement of air layer is regarded as a one-dimensional flow along the X-axis, and the equations of movement and continuity of air can be obtained.

$$\frac{\partial u}{\partial t} + u\frac{\partial u}{\partial x} = -\frac{1}{\rho_a}\frac{\partial p}{\partial x} \tag{3}$$

$$\frac{\partial(\rho_a h)}{\partial t} + u\frac{\partial(\rho_a u h)}{\partial x} = 0 \tag{4}$$

where u is the horizontal velocity of air layer, p is the pressure of air, ρ_a is the density of air, and h is the thickness of air layer.

When the buoy falls a certain distance from the surface of water, the air is compressed quickly because it has no time to be expelled. At the initial time $t = 0$, $h(x,t) = h_0$, $v(t) = v_0$, then the distance between flat structure and water surface can be expressed as:

$$h(x,t) = h_0 - w(x,t) - \int_0^t v(t)\,\mathrm{d}t \tag{5}$$

where $w(x,t)$ is the height of the free water surface.

According to the momentum theorem, the equations of velocity change of buoy under the action of gravity and the reaction of air can be obtained:

$$v(t) = v_0 + gt - \frac{1}{M_s}\int_0^t \mathrm{d}t \int_{-R}^{R}(p - p_0)\,\mathrm{d}x \tag{6}$$

where p_0 is the initial pressure of air, M_s is the mass of the flat bottom structure, and g is the acceleration of gravity.

When the buoy structure falls very close to the water surface, assuming that the air at this moment is no longer compressed and the disturbance of water surface waveform is ignored, $u(0,t) = 0$ can be obtained by using the separation of variables method and the conditions at the midpoint of bottom, and the flow velocity equation of air can be obtained by using the continuity Equation (2):

$$u(x,t) = -\frac{x}{h}v(t) \tag{7}$$

By substituting Equation (5) into the air motion Equation (3), and using the conditions $p(\pm R,t) = p_0$ at the flat edge, the pressure distribution can be obtained:

$$p(x,t) = p_0 + \rho_a\frac{R^2 - x^2}{h^2}\left[v^2 - \frac{h}{2}\frac{\mathrm{d}v}{\mathrm{d}t}\right] \tag{8}$$

As the buoy falls to the surface of water, the volume of air in groove is compressed, and the change in gas state can be approximated as an adiabatic process. In general, the actual gas is not significantly different from the ideal gas, so the gas in groove can be regarded as the ideal gas without affecting the accuracy.

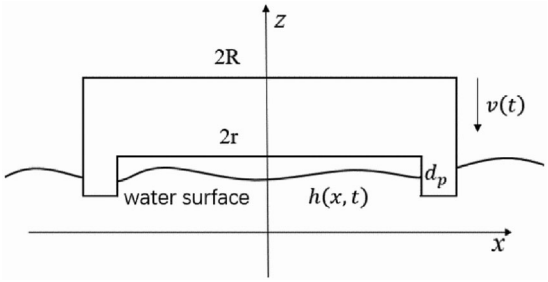

FIGURE 3 Simple buoy model when entering water

2.2 | Calculation of peak impact after water entry

The theoretical model of the air cushion of oscillating buoy when entering water is shown in the Figure 3. According to the equation of state of an ideal gas in aerothermodynamics:

$$(p + p_a)\ V^m = (p_0 + p_a)\ V_0^m \tag{9}$$

where p_a is one standard atmosphere, V is the real-time volume of the compressed gas, V_0 is the initial volume of gas, m is a variable index, which is 1.4 in the adiabatic process and 1 in the isothermal process.

When the bottom surface of buoy is flush with the water surface, assuming the time is t_1, the depth of groove is d_p, and the bearing area of water in the gas compression process is A_w, the initial volume of gas is:

$$V_0 = A_w\ d_p \tag{10}$$

The real-time volume is:

$$V = A_w\ (d_p - h(x,t) + h(x,t_1)) \tag{11}$$

From the above formula, the bearing capacity of hollow air cushion in the full water entry process can be derived:

$$f(x,t) = A_w\left[(p_0 + p_a)\left(\frac{d_p}{d_p - h(x,t) + h(x,t_1))}\right) - p_a\right] \tag{12}$$

It can be seen from Equations (8) and (12): During buoy drop into water, the impact pressure on the bottom of the buoy is closely related to the effective acting area of the buoy, which is closely related to the structure shape of the bottom of the buoy. Therefore, based on the cylindrical flat bottom buoy, we design air cushion with different structural sizes and shapes to investigate the influence of air cushion acting on buoy.

3 | THE INFLUENCE OF AIR CUSHION SHAPE ON THE IMPACT OF BUOY

3.1 | Basic principles of ALE algorithm

This paper uses LS-DYNA finite element software to simulate the problem of buoy entering water. The powerful fluid-solid coupling function of LS-DYNA is widely used in the analysis of large impact occasions. The core ALE algorithm can effectively deal with large deformation and element distortion problems.

In dealing with the large impact problem, the biggest difficulty is that the large deformation of structure may cause serious distortion of the finite element mesh and the turbulence or even termination of calculation process. The ALE algorithm solves this problem well. The difference between ALE algorithm and traditional Lagrange algorithm is that the ALE algorithm has two layers of grids. The spatial grid can move arbitrarily, and the deformation of material grid can be transported to the moving spatial grid. The Euler algorithm is in the middle of the two. It transports the deformation of material grid to a fixed spatial grid, not a moving spatial grid. Based on the ALE grid structure, the Euler-Lagrange coupling algorithm can be easily implemented in the LS-DYNA program, so as to realize the fluid-structure coupling calculation.

The simulation model in this article consists of three parts: buoy, water and air. All of them use the SOLID164 unit provided by LS-DYNA for finite element analysis. The discrete structural motion equation is:

$$M\ddot{x} = P - F + H - C\dot{x} \tag{13}$$

The solution process uses an explicit central difference method, and the basic format is as follows:

$$\ddot{x}\ (t_n) = M^{-1}\ \left[P\ (t_n) - F\ (t_n) + H\ (t_n) - C\dot{x}\left(t_{n-1/2}\right)\right] \tag{14}$$

$$\dot{x}\ \left(t_{n+1/2}\right) = \dot{x}\ \left(t_{n-1/2}\right) + \ddot{x}\,(t_n)\,(\Delta t_{n-1} + \Delta t_n)\,/2 \tag{15}$$

$$x\ (t_{n-1}) = x\,(t_n) + \dot{x}\left(t_{n+1/2}\right)\Delta t_n \tag{16}$$

where M is the overall mass matrix, P is the overall nodal load vector, F is the stress divergence vector, H is the hourglass viscous damping vector, and $x(t_n)$ is the nodal position coordinate vector at time t_n.

3.2 | Simulation model establishment

The shape and size of air cushion have a significant effect on the impact of buoy into water. For a better comparison, an air cushion is added at the bottom of buoy on the basis of the cylindrical buoy. Extract the two main size factors of air cushion: the water contact area, the depth of air cushion, and simplify the shape of air cushion into three types: short cylinder, long cylinder, and cone, and establish a flat-bottomed buoy (air cushion thickness is 0) as a model for the comparison group. Four types of buoy models as shown in Figure 4 are established, and the impact simulation is performed. Among them, the three air cushion buoys have the same volume. The base area of the short cylinder and the cone is the same, and the depth of the long cylinder and the cone are the same. Because these air-cushion buoys are all axisymmetric, the load received can also be regarded as axisymmetric, so they can be simplified into a two-dimensional model for research while meeting the accuracy requirements. It can greatly reduce the amount of calculation, and it is also conducive to meshing, operation and observation.

TABLE 1 Mesh independence verification

Degree	Number of meshes	Peak impact	Difference from fine mesh
coarse	62,883	585.55 kN	2.3%
medium	141,000	594.27 kN	0.8%
fine	288,579	599.02 kN	

The simulation model is shown in Figure 5. In order to simulate the actual situation, the size of buoy is the same as that of the damaged buoy in Figure 1. In the two-dimensional model, the overall size of the cylindrical buoy is set to Ø1000 mm × 600 mm. An air cushion is set at the bottom of buoy. The size of the short cylinder is Ø800 mm × 40 mm, and the size of the long cylinder is Ø800 mm × 40 mm. The size of the cone air cushion is Ø800 mm × 160 mm, that is, the bottom diameter is the same as the short cylinder air cushion, and the height is the same as the long cylinder.

In order to prevent the difference in the number of meshes from interfering with the calculation results, this paper uses multiple sets of meshes with different accuracy to verify the mesh independence. The verification scheme and detailed information are shown in Table 1. Under the same time step, the results of the coarse mesh are quite different from the other two, and the results of the medium and fine mesh are basically the same. Considering the calculation time, this simulation uses a medium mesh quality.

The simulation model includes three parts: Buoy, water and air. The buoy part is divided into 6000 Lagrange volume units, the material is set as a rigid body, the elastic modulus is 200 GPa, and the Poisson's ratio is 0.3. The water body is set as a non-viscous, compressible linear fluid, and the water area size is 3000 mm×2500 mm, divided into 75,000 Euler body units. The air domain is set as a compressible ideal gas, the size is 3000 mm×2000 mm, and the number of Euler body units is 60,000.

The pressure in the water region is described by a polynomial equation of state [21,22]:

$$p_{\text{water}} = \begin{cases} a_1\mu + a_2\mu^2 + a_3\mu^3 + (b_0 + b_1\mu)\,\rho_0 e & \textit{compression state}: \mu > 0 \\ a_1\mu + (b_0 + b_1\mu)\,\rho_0 e & \textit{tensile state}: \mu < 0 \end{cases} \tag{17}$$

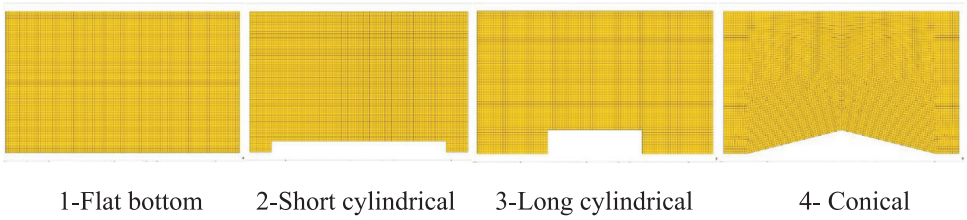

FIGURE 4 Buoy models of several air cushion shapes

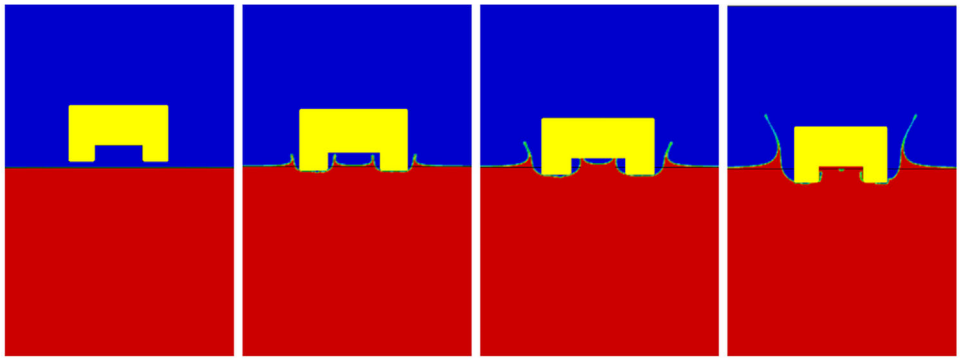

FIGURE 5 Simulation process of buoy entering water

In the formula, p is the pressure, $\mu = \rho_w/\rho_0 - 1$, ρ_w and ρ_0 are the density and reference density of water, respectively, and e is the internal energy per unit mass.

The pressure in the air region is described by the Gamma equation of state:

$$p_{\text{air}} = (\gamma - 1)\rho_a e_a \tag{18}$$

In the formula, γ is the specific heat capacity of gas, $\gamma = 1.401$, $\rho_a = 1.2\ \text{kg/m}^3$ at standard atmospheric pressure and room temperature, e_a is the internal energy of air, $e = 211.04\ \text{J/g}$.

The top surface of air part is set as a free inflow and outflow boundary, and the remaining surfaces are set as a non-reflective boundary. In the element boundary condition setting, all elements restrict the freedom of movement in the y-axis direction and the rotational freedom in the x-axis and z-axis directions. The air unit and the water unit share a node at the interface. The outer surface of buoy is defined as a fluid-solid coupling surface, using any Lagrangian–Euler (ALE) coupling algorithm, the nodes of Lagrangian and Euler grids coincide on the coupling surface. When Lagrange unit moves and deforms, the fluid-solid coupling surface moves accordingly, making the Euler unit move with it. In the calculation process, the fluid-solid coupling surface is the flow field boundary of the Euler unit, and the Euler unit exerts pressure on the boundary, making the buoy Lagrange unit subject to fluid load. Figure 5 shows the simulation of the change process of the buoy and the water during buoy entering water, and the change of air cushion can be clearly observed.

3.3 | Simulation analysis of air cushion's shape to reduce buoy water impact

According to the data from the buoy station in Xiangshan, Zhejiang, under the influence of Super Typhoon Lekima, the maximum wave height in the Xiangshan sea area is about 11 m, with a period of 10–12 s. The maximum impact velocity of the waves is about 7 m/s. In the simulation process, the initial water entry velocity of buoy is set to 10 m/s, the simulation calculation time is 0.05 s, and the sampling frequency is 5 kHz. Figure 6 shows the time history of impact force of the four types of buoys when they slam into water.

It can be seen from the figure that all four types of buoys start to enter water at $t = 18$ ms, and the impact force of the flat-bottomed buoy reaches the maximum peak value of 594.27 kN at $t = 20.6$ ms. The impact force of the short cylindrical air

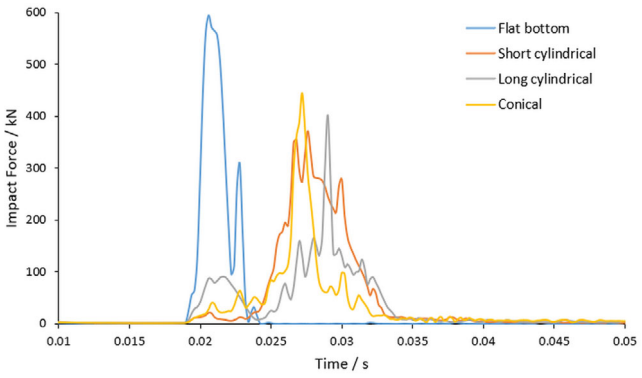

FIGURE 6 Time history of impact force of each buoy

FIGURE 7 Short cylindrical air cushion

FIGURE 8 Long cylindrical air cushion

cushion buoy reaches its peak at $t = 27.6$ ms, and the maximum impact force is 371.09 kN. The impact force of the long cylindrical air cushion buoy reaches its peak at $t = 29$ ms, and the maximum impact force is 401.57 kN. The impact force of the conical air cushion buoy reaches its peak at $t = 27.2$ ms, and the maximum impact force is 445.12 kN. The comparison with the flat bottom buoy shows that the buoy air cushion can greatly reduce the impact of water on buoy.

Comparing the impact time history curves of the four types of buoys, it can also be seen that the air cushion has a delay effect on the peak impact force received by buoy when it enters water, which is related to the thickness of air cushion. The greater the thickness, the more obvious the delay effect. The conical air cushion and the short cylindrical air cushion have a peak delay time of 7.2–7.6 ms, which is relatively close, while the long cylinder has a peak delay time of 8.4 ms. Analyzing the reasons, the air cushion changes after the three types of buoys enter water are shown in Figures 7–9. When the buoys enter water, the liquid reaches the bottom of air cushion successively, forming a water impact peak. Obviously, the liquid has the longest time to reach the top of the long cylindrical air cushion, so the peak delay time of its water impact force is the longest.

It can also be found from the figure that when the buoy enters water, the liquid forms an impact oscillation on the bottom of air cushion buoy, resulting in multiple peaks of impact force. The larger the area of the bottom of air cushion, the greater the number of peak impact forces. In Figures 7–9, the bottom area

FIGURE 9 Conical air cushion

FIGURE 10 Air cushion effect of flat bottom buoy

of the short cylinder is the largest, the volume of the airtight air cushion formed at the top is larger, and the volume of the side airtight air cushion is smaller. The airtight air cushion at the top is broken several times, forming multiple impacts, of which there are three close peaks of impact force. The area of the bottom of the long cylindrical air cushion is relatively small, and the volume of the top air cushion is close to that of the side air cushion, which causes the volume of the top air cushion to be relatively small, and the peak water impact force in the vertical direction becomes larger. When the cone air cushion buoy enters water, the water will converge along the wall to the centre, forming a large airtight air cushion at the top of cone, and multiple airtight air cushions on the side. The cone-shaped flow gathering effect causes the peak of impact force to increase when the water reaches the top of cone.

The above analysis shows that the horizontal cross-sectional area of the top airtight air cushion has a significant effect on the reduction of peak water impact force. The larger the cross-sectional area, the more obvious the effect of reducing the peak water impact force. Comparing several types of buoys, the short cylindrical air cushion has the largest cross-sectional area and the best impact reduction effect when entering water.

It must be pointed out here that at $t = 0.0228$ s, a small peak lagging behind the collision time is also produced on the curve of the flat bottom buoy. This is because there is still a small airtight cushion when the flat-bottomed buoy enters water, as shown in Figure 10. After the buoy enters water, the air escapes from both sides, causing the volume of air cushion to change, which leads to small fluctuations in the peak water impact force.

3.4 | Simulation analysis of air cushion volume to reduce buoy water impact

The volume of air cushion is an important factor affecting the impact resistance of air cushion buoy. The short cylindrical air cushion buoy with the best wave peak reduction effect is selected here, and the volume of air cushion is changed by changing the thickness of air cushion, and the water impact simulation is performed on the buoys with different air cushion volumes. The overall size of the buoy model is Ø1 m × 0.6 m. The depth of air cushion is set here from 0–0.35 m, increasing by 0.05 m each time. While keeping the mass and volume of buoy unchanged, the height of buoy will change with the depth of air cushion. In the simulation, the initial velocity of buoy into water is set to 10 m/s, the calculation time is 0.1 s, and the sampling frequency is 1 kHz. Figure 11 shows the impact force of

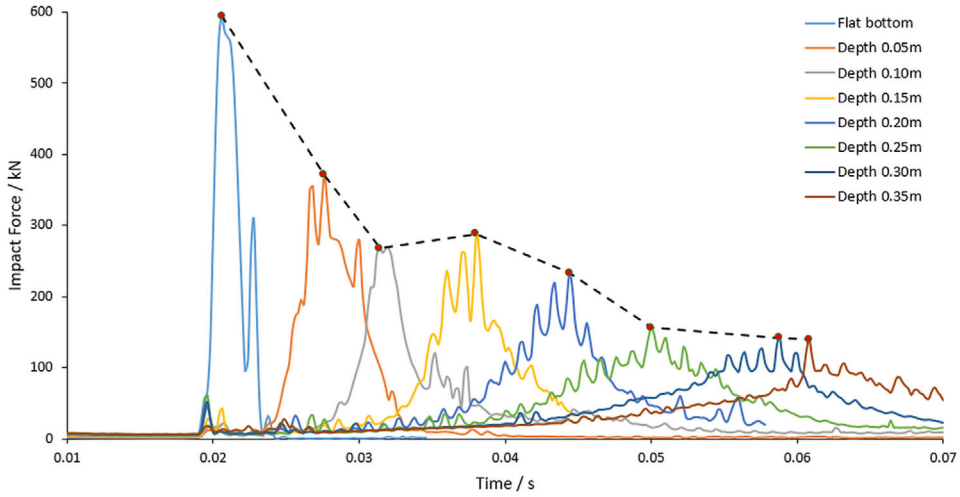

FIGURE 11 Time history of impact force of each buoy

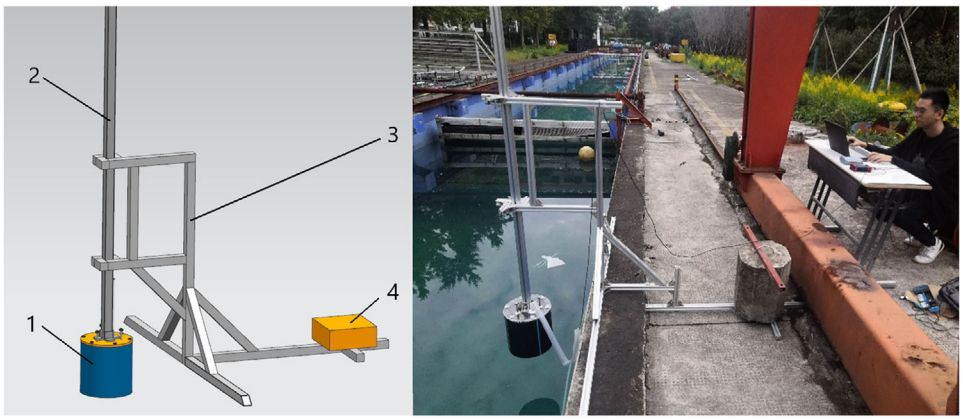

FIGURE 12 Buoy water impact test device

buoys with different air cushion depths in the process of entering water.

From the simulation results, it can be found that when the thickness of air cushion is 0 (i.e. flat bottom), the peak impact force on buoy is 594.27 kN, and when the thickness of air cushion increases to 50 mm, the impact force of water on buoy is 371.09 kN, and the peak impact force reduction rate reaches 37.6%. With the further increase of the thickness of air cushion, the peak impact force showed an overall downward trend, but after the thickness of air cushion increased to 250 mm, the peak impact force decreased not significantly.

Observe the time of peak impact. When the bottom is flat, the peak impact occurs at about 0.02 ms. Then, for every 50 mm increase in the thickness of air cushion, the peak impact time is 0.025, 0.032, 0.038, 0.045, 0.05, 0.058, and 0.061 ms. This shows that the air cushion has a delay in the time of peak impact. The thicker the air cushion, the more obvious the peak impact delay. After the air cushion thickness is increased to 250 mm, the delay phenomenon is not obvious. It can also be seen from the figure that, compared with flat-bottomed buoys, the air cushion buoy bears more than three peak impact forces after entering water. The greater the thickness of air cushion, the greater the number of peak impact forces of water on buoy. This is mainly due to the vibration inside the air cushion after buoy enters water to form an airtight air cushion.

4 | EXPERIMENTAL TEST AND VERIFICATION

4.1 | Construction of the experimental platform

Due to the limited experimental conditions, the experiment was carried out in a large pool using a scaled-down model. Figure 12 shows the test bench for the impact test of the oscillating buoy. In the figure, 1 is a cylindrical adjustable test buoy, the top of which is connected with the guide rod 2, and 3 is a bracket with a slide rail, and the counterweight 4 ensures the stability of test bench. The upper end of the buoy 1 is connected with a guide

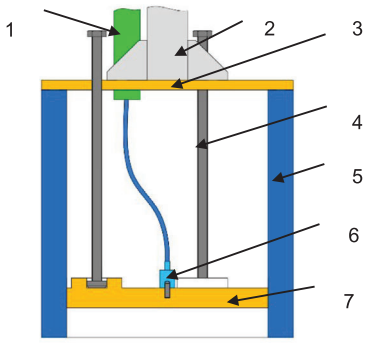

1. Wire protection hose 2. Guide rod 3. Cover plate 4. Adjustable support rod 5. Side wall 6. Acceleration sensor 7. Base plate

FIGURE 13 Buoy section structure

rod 2, and the guide rod 2 and the bracket 3 are connected by a linear slide rail to ensure the up and down sliding direction determined by the guide rod. At the same time, a scale is set on the guide rod to accurately locate the initial position of buoy. The top of the guide rod is connected with the hook of the upper bridge crane with a string. Cut the string, the guide rod and the buoy will hit water vertically downward along the slide rail. In the experiment, the drop height can be changed between 0.1 and 1 m.

The overall structure size of the buoy model is Ø250 mm × 300 mm. The internal cross-sectional structure is shown in Figure 13. 1 is the protective wire hose, which is the lead waterproof protective tube of the acceleration sensor 6. The disc-shaped cover 3, the hollow cylindrical wall 5 and the cylindrical bottom plate 7 constitute the buoy body. The bottom plate 7 is at a certain distance from the bottom of the cylinder wall 5. After the cylinder wall 5 enters water, the gap between the cylinder wall and the bottom plate 7 forms an air cushion. The bottom plate can slide up and down along the inner wall of 5 through the adjusting screw 4 to achieve the purpose of adjusting the volume of air cushion. The IEPE piezoelectric acceleration sensor is used here to measure the impact force, with a measuring range of 100 g and a measuring frequency of 5000 Hz. The acceleration sensor is installed on the buoy bottom plate through M5 bolts. The constant current adapter model used is CT5201, and the USB-1608G data acquisition card and TracerDAQ software are used for data acquisition and processing.

In addition to gravity mg (m is the mass of buoy, g is the acceleration of gravity), the buoy is also subject to the reverse impact force F_{impact} of water on the buoy during the entry into water. Calculate the impact force of buoy through the measured acceleration a of buoy: $F_{impact} = m(a + g)$. Thus the impact curve of buoy into water is obtained.

4.2 | Experiment and analysis of air cushion shape to reduce buoy water impact

During the experiment, the initial height of buoy from water surface can be adjusted to obtain different initial velocities. The initial height of buoy is set here, so that the corresponding water entry velocity is 2.5 m/s. Measure the impact force of four types of buoys: Flat bottom, short cylindrical air cushion, long cylindrical air cushion, and conical air cushion when entering water. Figure 14 shows the water impact time history curves of four types of buoys. It can be seen from the figure that the impact occurs in 7–8 ms when the buoy enters water. However, the maximum impact peak appearance time is about 8 ms for the flat-bottomed buoy, and the maximum peak appearance time of the other three buoys is very close, about 11 ms, which is similar to the simulation result (Figure 11). In the figure, the impact force has a negative value of oscillation, which is caused by the vibration of the sensor due to impact.

The time history curves of the water impact force of the four buoys are extracted here. As shown in Figure 14, the curves (a), (b), (c), (d) correspond to the water impact peaks of the four types of buoys: flat bottom, conical air cushion, long cylindrical air cushion, and short cylindrical air cushion. Curve (a) has a single impact force peak with a peak value of 9.094 kN, and curve (b) has three impact force peaks, which are 4.363, 7.202, and 3.963 kN, with an interval of 3–5 ms; curve (c) has three impact force peaks, which are 6.065, 6.456, and 4.070 kN, and the interval time is 3–10 ms; curve (d) has three impact force peaks, which are 4.094, 5.852, and 1.550 kN respectively. Set buoy (a) as a rigid buoy, use this as a benchmark, and define the peak reduction coefficient of air cushion buoy as (the peak impact force of the rigid buoy-the peak impact force of air cushion buoy)/the peak impact force of the rigid buoy. The peak reduction coefficients of buoys (b), (c), and (d) are 0.208, 0.29 and 0.357 respectively. Obviously, the peak reduction coefficient of buoy 4 is the largest. That is to say, the peak reduction effect of the short cylindrical air cushion buoy is the best, which is consistent with the simulation trend.

It is also noticed here that there are 2–3 obvious peaks in curves (b), (c), and (d). Comparing several peaks, we can find that the second peak is the largest. Analysis of the reason is that when the buoy starts to enter water, the bottom of buoy wall has an impact when it just enters water. The bottom area of wall is relatively small, so the impact is small. After the bottom is completely filled with water, a closed air cushion is formed. A larger impact peak occurs again when the air cushion is broken, which is consistent with the simulation results.

Comparing curves (b), (c) and (d), it can be seen that the impact curve of the short cylindrical air cushion buoy is smoother and the impact peak value is lower, which indicates that the larger the relative area of buoy air cushion in contact with water, the more obvious the impact peak reduction effect. The time interval between the first two impact peaks of the short cylindrical air cushion buoy is about 3ms, and the time interval between the first two impact peaks of the long cylindrical air cushion buoy is about 5ms, and the time interval is longer. The main reason for this is that when a secondary impact occurs, the time for the short cylindrical air cushion to reach the top of air cushion cavity along the impact direction is shorter than that of the long cylindrical air cushion buoy. This is also consistent with the simulation results.

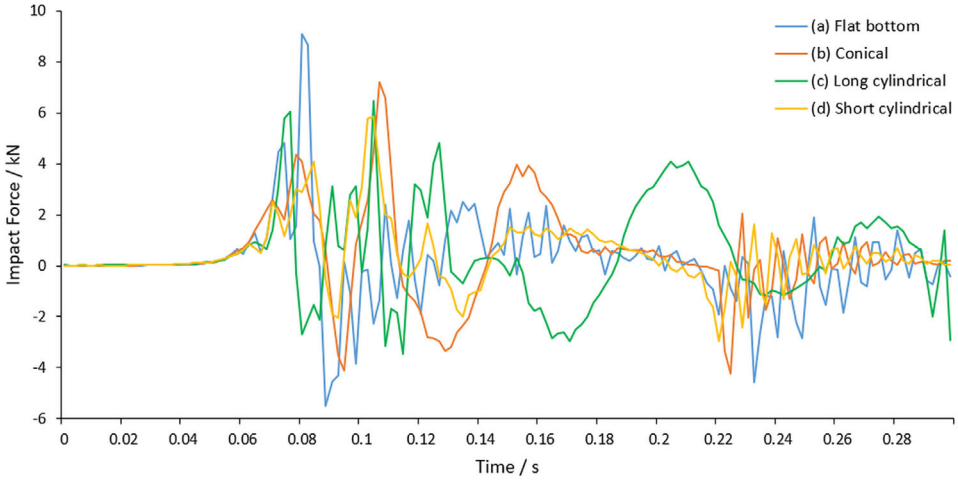

FIGURE 14 Comparison of the water impact force of each buoy

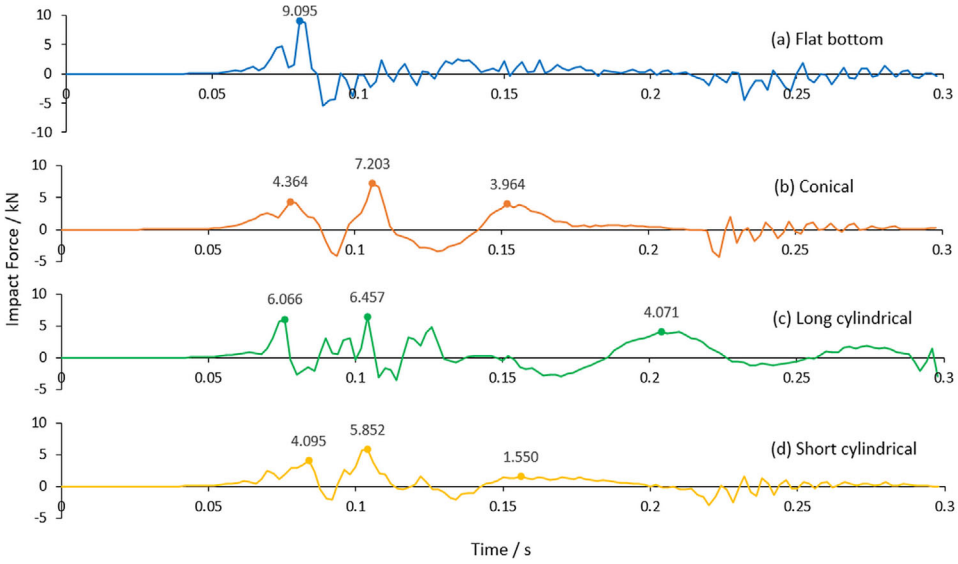

FIGURE 15 Water impact force of buoys with different air cushion shapes

4.3 | Experiment of the impact effect of the buoy at different entry velocities

During the experiment, adjusting the initial height of buoy from water surface can obtain different initial velocities of entering water. Five groups of different initial heights of buoys are set here, and the corresponding water entry velocities are 1, 1.5, 2, 2.5 and 3 m/s. The impact acceleration of four kinds of buoys entering water at different velocities was measured, and each set of experiments was repeated three times. Figure 13 shows the water impact time history curves of four types of buoys. Take the average value of the acceleration peak values measured three times, and then convert the average value of the acceleration peak values into the impact force received by buoy, and the result is shown in Figure 15. Curves (a), (b), (c) and (d) in the figure correspond to the water impact peaks of the four types of buoys: flat bottom, conical air cushion, short cylindrical air cushion, and long cylindrical air cushion.

It can be seen from the Figure 16 that with the increase of the initial water entry velocity, the greater the impact force on the four types of buoys. Among them, the peak of impact force received by buoy (a) (flat bottom buoy) is obviously greater than that of the other three types of buoys. With the increase of the initial water entry velocity, the difference in impact force becomes more obvious, which indicates that the air cushion at the bottom of buoy has a significant impact reduction effect.

Continuing to compare curves (b), (c) and (d), it can be seen that the impact force values of the three buoys are close when the water entry velocity is 1-1.5m/s. As the initial water entry velocity increases, the water impact peak reduction effect of the three buoy air cushions is better. At the same time, as the

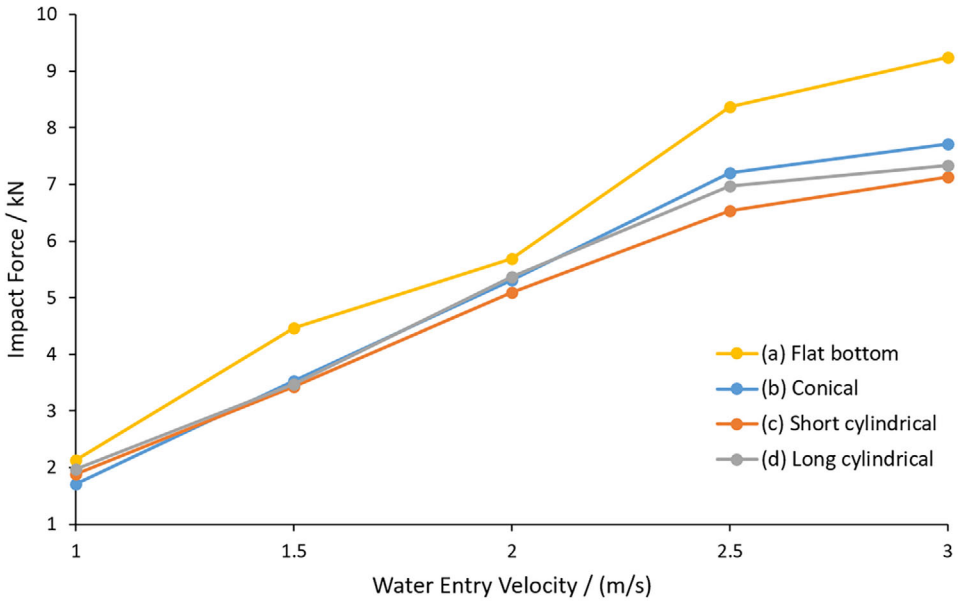

FIGURE 16 The maximum impact force of several types of buoys at different velocities

initial water entry velocity increases, the impact reduction effect of the three types of buoy air cushions is more obvious. The short cylindrical air cushion buoy has the best effect in reducing the peak water impact force, which is consistent with the simulation results.

4.4 | Experiment and analysis of air cushion volume to reduce buoy water impact

The buoy model shown in Figure 13 is used. An adjustable circular plate is placed inside a cylindrical cavity to form an air cushion, and the distance between the circular plate and the bottom of cylinder is adjusted by adjusting the screw to achieve the purpose of adjusting the volume of air cushion. During the experiment, the same buoy was tested repeatedly at the same water entry velocity for three times. Then the maximum peak value of each acceleration curve is extracted, and the peak value of the three repeated experiments is averaged and substituted into the formula, and the obtained value is used as the final maximum impact force of buoy. In the experiment, the main conditions are the thickness of buoy air cushion and the water entry velocity. The water entry velocity is set from 1 to 3 m/s, and the thickness of the air cushion varies from 0–100 mm, with an increment of every 20 mm. There are six types of buoys in total. Figure 17 shows the water impact force curves of six groups of buoys at different entry velocities.

It can be seen from the figure that the peak value of the impact force of the six types of buoys increases with the increase of the water entry velocity, basically showing a linear relationship. The impact force reduction coefficient also increases with the increase of the water entry velocity. For example, the water impact peak reduction coefficient of a buoy with a thickness of 20 mm is increased from 0.18 to 0.50. At the same time, the greater the thickness of air cushion, the greater the reduction coefficient of the peak impact force of buoy. When the initial water entry velocity of buoy is within 2 m/s, and the thickness of air cushion exceeds 40 mm, the peak impact force basically remains at about 2 kN, which shows that the peak impact force of buoy is hardly affected by the thickness of air cushion at this time. This indicates that after the thickness of air cushion is increased to a certain extent, increasing the thickness of air cushion has no obvious effect on the reduction coefficient of the peak impact force. This is consistent with the trend of simulation results.

Figure 18 shows the impact force curves of four types of buoys with air cushion thicknesses of 0, 20, 80, and 100 mm when the water entry velocity is 3 m/s, and they are listed respectively in Figure 19. Comparing with Figure 13, it is found that the impact force has a negative value. The reason is that during the process of entering water, due to the overall elastic structure of buoy, it oscillates after being impacted, which leads to a negative value when the acceleration sensor measures. Ignoring the negative value here, it can also be observed that the flat bottom buoy has a very large impact force peak, but there is no second and third peak; while the buoy with air cushion thickness has three main impact force peak. The water impact peak reduction coefficients of the three air cushion thickness buoys are 0.286, 0.518, and 0.629. This proves that the thicker air cushion, the more obvious the reduction effect of the water impact peak, which is consistent with the simulation results. At the same time, it can be seen from the figure that the thicker air cushion, the more obvious the delay to the peak impact force, and the trend is also consistent with the simulation results.

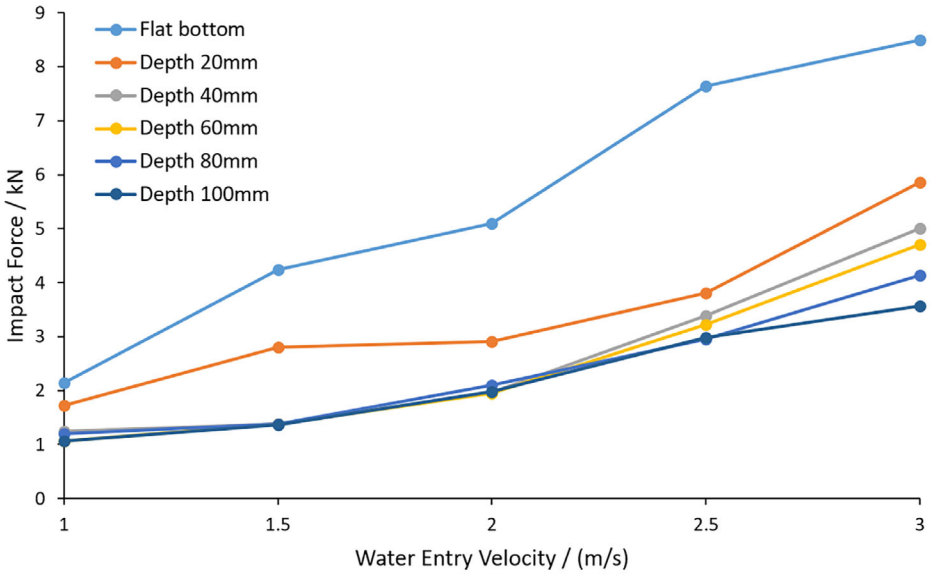

FIGURE 17 The maximum impact force of each buoy at different velocities

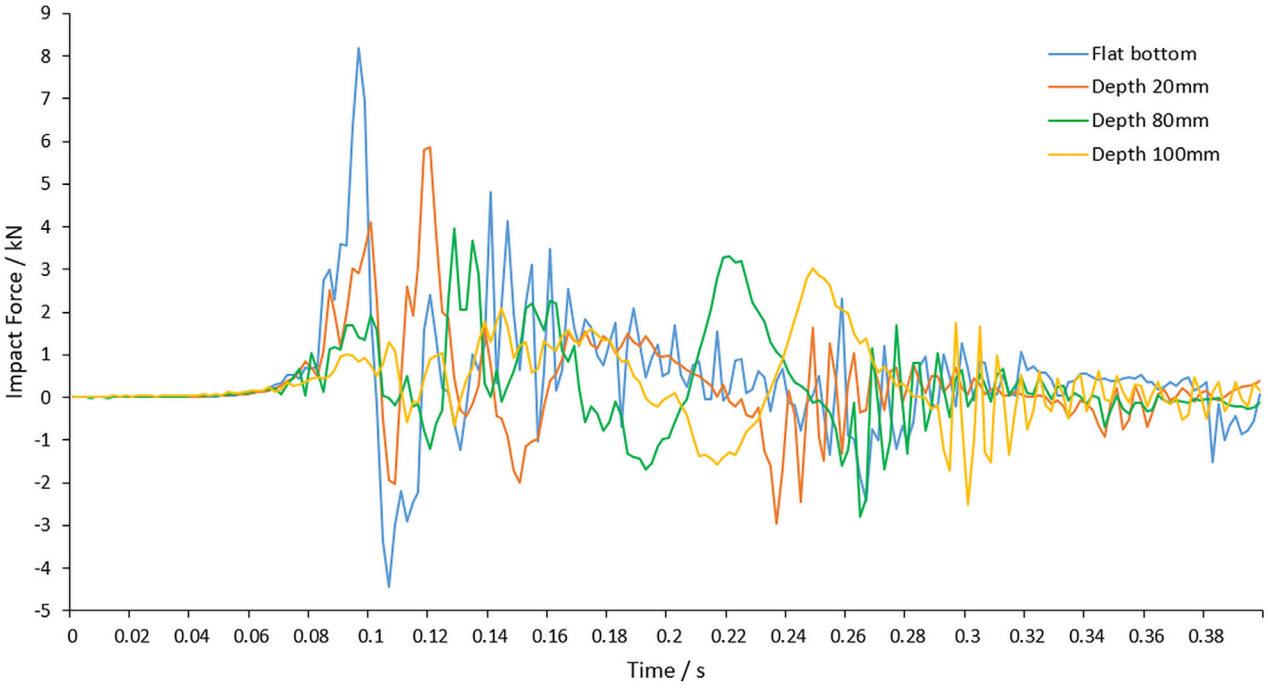

FIGURE 18 Comparison of water impact force of each buoy

5 | CONCLUSION

In this paper, the impact process of buoy with air cushion is studied, and the influence of the shape and volume of air cushion on the impact force of buoy is analysed. The main conclusions are as follows:

1. The peak value of the impact force of buoy increases with the increase of water entry velocity, basically showing a linear relationship. Compared with flat bottom buoy, the impact force of buoys with air cushions is greatly reduced. And with the increase of initial water entry velocity, the difference in impact force becomes more obvious, which indicates that the air cushion at bottom of buoy has a significant impact reduction effect.
2. When the buoy enters water, the liquid forms an impact oscillation on the bottom of air cushion buoy, resulting in multiple peaks of impact force, which reduces the peak

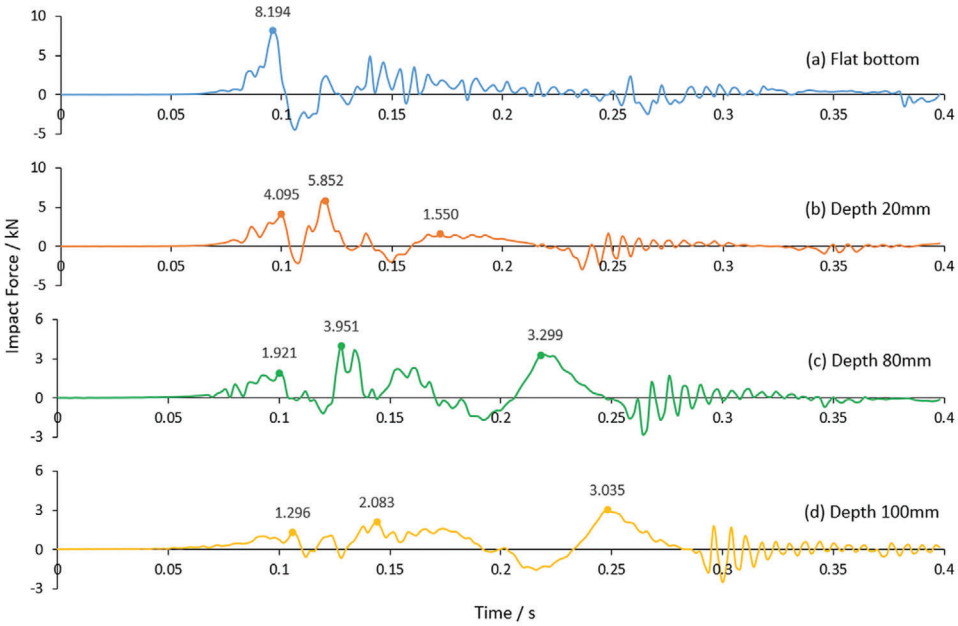

FIGURE 19 Water impact force of buoys with different air cushion volumes

value of impact force. The larger the area of the bottom of air cushion, the greater the number of peak impact forces. Therefore, the horizontal cross-sectional area of the top air-tight air cushion has a significant effect on the reduction of the peak water impact force. The larger the cross-sectional area, the more obvious the effect of reducing the peak water impact force. Comparing several types of buoys, the short cylindrical air cushion has the largest cross-sectional area and the best impact reduction effect when entering water.

3. The volume of air cushion is an important factor affecting the impact resistance of air cushion buoy. With the volume of air cushion increases, the peak impact force shows an overall downward trend, but the rate of decline gradually slows down. When the volume of air cushion increases to a certain value, the peak impact force decreased not significantly, and this value is positively correlated with the impact velocity of buoy.
4. The air cushion has a delay effect on the peak impact force received by buoy when it enters water, which is related to the volume of air cushion. The larger the volume, the more obvious the delay effect. However, when the volume of air cushion increases to a certain value, the delay phenomenon is not obvious, and this value is also positively correlated with the impact velocity of buoy.

Due to time and experimental conditions, the study on the impact of buoys into water still has some deficiencies. This paper studies the situation where the oscillating buoy enters water in a direction perpendicular to the water surface, but in real sea conditions, the impact of waves on buoy has a certain horizontal component, which should be studied in the future. Moreover, this paper only conducted experiments with a scaled-down model in a large pool. In the future, it is necessary to conduct field experiments at sea.

FUNDING

National Key R&D Program of China (No. 2016YFC0300500) Major Science and Technology Research Projects of Ningbo (No: 2017C110005) the Scientific and Technological Major Project of Ningbo (2015C50061).

ACKNOWLEDGEMENTS

The paper was supported by National Key R&D Program of China (No. 2016YFC0300500), Major Science and Technology Research Projects of Ningbo (No: 2017C110005), and the Scientific and Technological Major Project of Ningbo (2015C50061).

ORCID

Ruiyin Song https://orcid.org/0000-0001-8271-0441

REFERENCES

1. O'Sullivan, D.L., Lewis, A.W.: Generator selection for offshore oscillating water column wave energy converters. In: 13th International Power Electronics and Motion Control Conference, Poznań, Poland (2008)
2. Whittaker, T., Folley, M.: Nearshore oscillating wave surge converters and the development of Oyster. Philos. Trans. 370(1959), 345–364 (2012)
3. Huang, S., et al.: Experimental Study on interaction between degrees of freedom in a wave buoy. J. Ocean Univ. China 18(6), 1256–1264 (2019)
4. Alamian, R., et al.: Evaluation of technologies for harvesting wave energy in Caspian Sea. Renewable Sustainable Energy Rev. 32(5), 468–476 (2014)
5. Wu, B., et al.: Study on two optimizing methods of the oscillating type wave energy conversion devices. Acta Energiae Solaris Sinica 31(6), 769–774 (2011)
6. Jean-Roch, N., et al.: Hydrodynamic and energetic properties of a finite array of fixed oscillating water column wave energy converters. Ocean Eng. 88, 131–148 (2014)

7. Song, R., et al.: Experimental test study of wave energy generation system with catamaran platform. Acta Energiae Solaris Sinica 72, 318–330 (2019)
8. Michael, E., Mccormick.: Ocean wave energy conversion. Renewable Energy 1(11), 1309–1319 (1986)
9. Dalton, G.J., et al.: Case study feasibility analysis of the Pelamis wave energy convertor in Ireland, Portugal and North America. Renewable Energy 35(1), 443–455 (2010)
10. Bar-Avi, P., Benaroya, H.: Nonlinear dynamics of an articulated tower in the ocean. J. Sound Vib. 190(1), 77–103 (1996)
11. Tiron, R., et al.: The challenging life of wave energy devices at sea: A few points to consider. Renewable Sustainable Energy Rev. 43, 1263–1272 (2015)
12. Yemm, R., et al.: Pelamis: Experience from concept to connection. Royal Soc. Math. Phys. Eng. Sci. 370(1959), 17 (2012)
13. Paik, J.K., Thayamballi, A.K.: A concise introduction to the idealized structural unit method for nonlinear analysis of large plated structures and its application. Thin-Walled Struct. 41(4), 329–355 (2003)
14. Masanori, T., et al.: Comparison of the performance of mask ventilation between face masks with and without air cushion. J. Oral Maxillofacial Surg. 77(12), 2465 (2019)
15. Wen, J., et al.: Exploiting air cushion effects to optimise a superhydrophobic/hydrophilic patterned liquid ring sealed air bearing. Tribol. Int. 144, 106129 (2019)
16. Antonutti, R., Hearn G.E.: Optimisation of point-absorber arrays. In: 9th European Wave and Tidal Energy Conference (EWTEC), Southampton (2011)
17. Cole, R.E., Neu, W.L.: Validation of a commercial fluid-structure interaction solver with applications to air cushion vehicle flexible seals. Ocean Eng. 189(10), 106287 (2019)
18. Ji, R., et al.: Array characteristics of oscillating-buoy two-floating-body wave-energy converter. J. Mar. Sci. Appl. 18(3), 325–333 (2019)
19. Salumäe, T., Kruusmaa, M.: A flexible fin with bio-inspired stiffness profile and geometry. J. Bionic Eng. 8(4), 418–428 (2011)
20. Khabakhpasheva, T.I., Korobkin, A.A.: Elastic wedge impact onto a liquid surface: Wagner's solution and approximate models. J. Fluids Struct. 36(4), 32–49 (2013)
21. Li, W.P., et al.: Elasticity effects on the water impact of an elastic flat- bottom box. J. Hydrodyn. 14(2), 64–70 (2002)
22. Bereznitski, A.: Slamming: The role of hydroelasticity. Int. Shipbuild. Prog. 48(4), 333–351 (2001)

How to cite this article: Song, R., et al.: The study on the anti-impact performance of the oscillating buoy with various air cushions. IET Renew. Power Gener. 15, 3459–3471 (2021). https://doi.org/10.1049/rpg2.12183